scientific reports

Check for updates

OPEN

Quantitative separation of CEST effect by R_{ex}-line-fit analysis of Z-spectra

Gang Xiao[1,6], Xiao-Lei Zhang[2,6], Si-Qi Wang[3], Shi-Xin Lai[3], Ting-Ting Nie[4], Yao-Wen Chen[3], Cai-Yu Zhuang[2], Gen Yan[5]✉ & Ren-Hua Wu[2]✉

The process of chemical exchange saturation transfer (CEST) is quantified by evaluating a Z-spectra, where CEST signal quantification and Z-spectra fitting have been widely used to distinguish the contributions from multiple origins. Based on the exchange-dependent relaxation rate in the rotating frame (R_{ex}), this paper introduces an additional pathway to quantitative separation of CEST effect. The proposed R_{ex}-line-fit method is solved by a multi-pool model and presents the advantage of only being dependent of the specific parameters (solute concentration, solute-water exchange rate, solute transverse relaxation, and irradiation power). Herein we show that both solute-water exchange rate and solute concentration monotonously vary with R_{ex} for Amide, Guanidino, NOE and MT, which has the potential to assist in solving quantitative separation of CEST effect. Furthermore, we achieve R_{ex} imaging of Amide, Guanidino, NOE and MT, which may provide direct insight into the dependency of measurable CEST effects on underlying parameters such as the exchange rate and solute concentration, as well as the solute transverse relaxation.

Keywords Chemical exchange saturation transfer, Quantitative separation, R_{ex}-line-fit, Z-spectra

Chemical exchange saturation transfer (CEST)-magnetic resonance imaging (MRI) is a new contrast enhancement technique that indirectly measures molecules with exchangeable protons and exchange-related properties, providing high detection sensitivity[1–4]. In practice, the saturation transfer effects of CEST-MRI are often assessed and quantified using a Z-spectra where the water signal is plotted as a function of the applied saturation frequency. For in vivo CEST-MRI, proper parameter quantifications demand careful measurement of the CEST effects (uncontaminated and with sufficient SNR) such as solute concentration and solute-water exchange rate, thus rendering quantitative CEST a challenging task[5].

Theoretically, the CEST parameter quantification through Z-spectra fitting demonstrated by Bloch-McConnell (BM) equations could provide a feasible approach, and yet there are the common problems of slow operation speed and converging to local optimal solution. Nevertheless, scholars spent their efforts and carried on studies of CEST quantification in another way. The symmetric magnetization transfer ratio (MTR_{asym}) that calculated from a Z-spectra is the most used CEST quantification method[6–8]. However, MTR_{asym} is confounded by several types of contamination, including direct saturation (DS), semisolid macromolecular magnetization transfer (MT) and nuclear Overhauser effect (NOE)[9,10].

To further boost CEST specificity, Z-spectra fitting has been successfully applied to differentiate the contributions from multiple origins[11], such as multiple-pool Lorentzian fit[12–14], the Lorentzian difference (LD) analysis[15,16], and three-point method[11,12]. For a specific solute along with overlapping signals from nearby pools, the LD analysis that employs a single Lorentzian line may not provide an accurate reference signal[10,16]. The same problem would still occur for a three-point method that relies on two nearby signals as a reference. The multiple-pool Lorentzian fit strongly relies on assumption that each CEST signal can be approximated as a Lorentzian lineshape[17].

Recent advancements in the quantification methods of CEST and NOE techniques have significantly improved their application in biomedical imaging, particularly in the context of brain tumors detection[18–22]. For example, Glang et al. proposed a deep neural network with uncertainty quantification that can efficiently and accurately

[1]School of Mathematics and Statistics, Hanshan Normal University, Chaozhou 521041, China. [2]Department of Radiology, Second Affiliated Hospital of Shantou University Medical College, Shantou 515041, China. [3]College of Engineering, Shantou University, Shantou 515063, China. [4]Department of Radiology, Hubei Cancer Hospital, Tongji Medical College, Huazhong University of Science and Technology, Wuhan 430079, China. [5]Department of Radiology, Second Affiliated Hospital of Xiamen Medical College, Xiamen 361021, China. [6]These authors contributed equally: Gang Xiao and Xiao-Lei Zhang. ✉email: gyan@stu.edu.cn; cjr.wurenhua@vip.163.com

predict Lorentzian parameters from CEST MRI spectra, providing fast and reliable CEST contrast image reconstruction while indicating prediction trustworthiness[18]. Cui et al. proposed a new method termed as 2π-CEST to reduce the contribution from APT in detecting NOE, offering a more accurate strategy than the conventional asymmetric analysis[20]. The study concludes that NOE (− 3.5 ppm) serves as a highly sensitive MRI contrast for imaging membrane lipids in the brain, with lipids being the primary contributor to NOE (− 3.5 ppm) signals, rather than proteins, explaining variations in signals between tumors, gray matter, and white matter[21].

Theoretically, the CEST specificity through Z-spectra rely on the pool size, exchange rate and relaxation time, as described by BM equations. Particularly, the exchange-dependent relaxation rate in the rotating frame (R_{ex}) that solved from the BM equations by an eigenspace approach, operates independently of non-specific tissue parameters and depends on specific parameters (solute concentration, solute-water exchange rate, solute transverse relaxation and irradiation power), therefore it is able to make the CEST more specific[2,4,16].

In this paper, a voxel-wise R_{ex}-line-fit method is developed to improve the reliability of Z-spectra fitting and investigate the potential of quantitative separation (Fig. 1), in which the simulation of a 5-pool model is used to complement the program capabilities. Our study first elucidates the relationship between R_{ex} and parameters such as solute concentration, solute-water exchange rate and $T_{2,s}$. Then the R_{ex} imaging of Amide, NOE (− 3.5 ppm), Guanidino and MT is achieved by our method. Finally, we apply the R_{ex}-line-fit to study CEST effect in a brain tumor model, and the performance of this method in fitting quality is evaluated.

Materials and methods

Exchange-dependent relaxation rate in the rotating frame (R_{ex})

The resulting solution for the Z-spectra can be described by the monoexponential decay of the z-magnetization as a function of time with the rate $R_{1\rho}$[2]

$$Z(\Delta\omega, t_{sat}) = \left(P_{zeff}P_zZ_i - Z^{ss}(\Delta\omega)\right)e^{-R_{1\rho}(\Delta\omega)t_{sat}} + Z^{ss}(\Delta\omega) \tag{1}$$

where P_{zeff} is the projection factor on z-axis of the effective frame, t_{sat} is saturation time.

In the case of steady-state, the resulting solution for the Z-spectra at each offset $\Delta\omega$ simplifies to[23,24]

$$\frac{1}{Z^{ss}(\Delta\omega)} = \frac{1}{\cos^2\theta R_{1w}}R_{1\rho}(\Delta\omega) = \frac{1}{\cos^2\theta R_{1w}}(R_{eff}(\Delta\omega) + R_{ex.1}(\Delta\omega) + R_{ex.2}(\Delta\omega) + \cdots + R_{ex.n}(\Delta\omega)) \tag{2}$$

where Z^{ss} is the steady-state condition,R_{1w} denotes the longitudinal relaxation rate of water, and $\theta = \tan^{-1}\left(\omega_1/\Delta\omega\right)$ where $\omega_1 = \gamma B_1$ is the amplitude of the RF field. The R_{eff} which describes the relaxation of free water in the rotating frame can be approximated by

$$R_{eff}(\Delta\omega) = R_{1,w}\cos^2(\theta) + R_{2,w}\sin^2(\theta) \tag{3}$$

Further, the R_{ex} at a particular off-resonant frequency $\Delta\omega$ for a general exchanging pool i is[2]

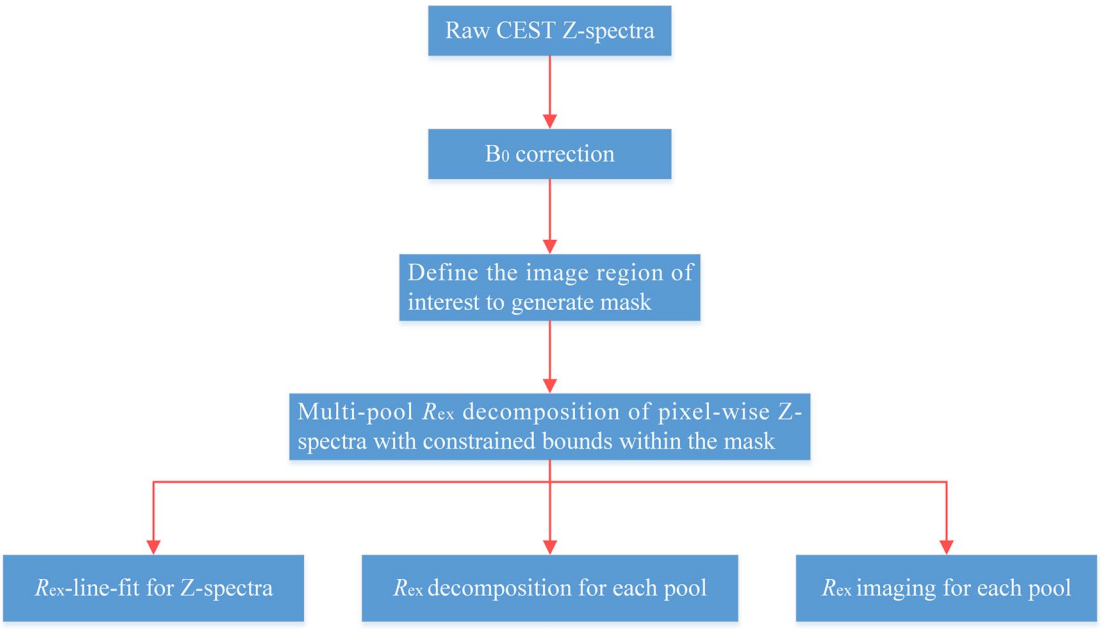

Fig. 1. Flow chart of data processing steps of R_{ex} based approach.

$$R_{\mathrm{ex}}(f_i,k_i,R_{2,\mathrm{i}}) = \underbrace{f_i k_i \underbrace{\frac{\delta\omega_i^2}{\omega_1^2+\Delta\omega^2}}_{\text{a - peak}} \underbrace{\frac{\omega_1^2}{\Gamma_i^2/4+\Delta\omega_i^2}}_{\text{b - peak}}}_{k_i\text{ - term}} + \underbrace{f_i R_{2,\mathrm{i}} \frac{\omega_1^2}{\Gamma_i^2/4+\Delta\omega_i^2}}_{R_{2,i}\text{ - term}} + \underbrace{f_i k_i \sin^2\theta \frac{R_{2,\mathrm{i}}(R_{2,\mathrm{i}}+k_i)}{\Gamma_i^2/4+\Delta\omega_i^2}}_{\text{corss - term}} \tag{4}$$

where f_i is a fraction of the total proton for the i^{th} pool,k_i is its exchange rate with water in Hz,$R_{2,\mathrm{i}}$ is its transversal relaxation rate,$\delta\omega_i$ is its frequency offset in Hz,$\Delta\omega_i$ is the difference in Larmor frequency between pool i and water, and the full width half maximum Γ_i is

$$\Gamma_i = 2\sqrt{\frac{R_{2,\mathrm{i}}+k_i}{k_i}\omega_1^2 + (R_{2,\mathrm{i}}+k_i)^2} \tag{5}$$

Multiple-pool Lorentzian-line-fit

To estimate CEST effects from individual components, we performed the multiple-pool Lorentzian fitting of Z spectra using a non-linear optimization algorithm[25]:

$$S(\Delta\omega)/S_0 = 1 - \sum_{i=1}^{N} L_i(\Delta\omega) \tag{6}$$

where

$$L_i(\Delta\omega) = \frac{A_i}{1+\frac{(\Delta\omega-\Delta_i)^2}{(0.5W_i)^2}} \tag{7}$$

Equation (7) represents a Lorentzian line with central frequency offset from water (Δ_i), peak FWHM (W_i), and peak amplitude (A_i). The value of N is the number of fitted pools; S is the measured signal on the Z-spectra; and S_0 is the non-irradiation control signal.

In this study, a five-pool model of Lorentzian-line-fit including Amide at 3.5 ppm (L_1), Guanidyl/Amine at 2.0 ppm (L_2), Water at 0 ppm (L_3), MT at − 2.4 ppm (L_4), and NOE at − 3.5 ppm (L_5) was performed to estimate CEST effects from individual components.

In vivo MR imaging

All animal care and experimental procedures comply with the National Research Council Guide for the Care and Use of Laboratory Animals. All animal experiments were approved by the Ethics Committee of Shantou University Medical College (Approval ID: SUMC2022-204) and conducted in accordance with the ARRIVE guidelines.

For our study, we used 8-week-old male SD rats (Beijing Vital River Laboratory Animal Technology Co., Ltd.) weighing approximately 250 g to establish a tumor-bearing model. In this study, three rats were prepared, where two rats were excluded from the present study due to tumor modeling failure that could not be used during data analysis. To implant the rat glioma C6 cells, a 10 µL suspension containing approximately 2×10^6 cells was injected into the right basal ganglia of the rats using a Hamilton syringe and a 30-gauge needle. After two weeks of tumor cell implantation, the rats underwent MRI. During the MRI procedure, the rats were anesthetized with a mixture of isoflurane and O_2 at a rate of 1 L/min. Anesthesia induction was achieved using 4.0% isoflurane, followed by maintenance anesthesia with 2.0–3.0% isoflurane. To monitor the breath rate, a respiratory probe was utilized throughout the MRI experiments. The rats' respiration rate and body temperature during the 7 T scan were maintained at approximately 60–70 breaths per minute and 38.5–39.5 °C, respectively.

MRI was conducted using a 7T horizontal bore small animal MRI scanner (Agilent Technologies, Santa Clara, CA, USA) equipped with a surface coil (Timemedical Technologies, China) for both transmission and reception. The positioning of the rat was carefully done to ensure that the tumor was accurately centered within the magnetic field. Imaging parameters were as follows: B_1 = 1 µT, repetition time (TR) = 6000 ms, echo time (TE) = 40 ms, array = frequency offsets, slice thickness = 2 mm, field of view (FOV) = 64 × 64 mm, matrix size = 64 × 64, spatial resolution = 1 × 1 mm, averages = 1. An echo planar imaging (EPI) readout sequence was employed to acquire CEST images, utilizing continuous wave (CW) RF irradiation on the scanners. The saturation time was set to 5.0 s, with 49 frequency offsets evenly distributed from − 6 to 6 ppm relative to the resonance frequency of water.

Results

To assess the performance of the proposed R_{ex}-line-fit, simulated Z-spectra are created using 5-pool system. The R_{ex} fitting is conducted by using a non-linear least square constrained optimization algorithm and referencing the pool parameters[1,26,27] in Table 1. Pseudo-code of our method for R_{ex} imaging and Z-spectra fitting is shown Table 2. The proposed R_{ex} fitting is compared experimentally to AREX[28] and multiple-pool Lorentzian fit[25]. The AREX is a reduced form of R_{ex} and follows a Lorentzian function[28], so the same parameters listed in Table 2 is used. Table 3 lists the boundaries of the multiple-pool Lorentzian fit[25].

Parameter separation

It is worthwhile to evaluate the correlation between R_{ex} and parameters (solute-water exchange rate k_s, solute concentration f_s and solute transverse relaxation $T_{2,s}$), which may assist in elucidating the R_{ex} specificity and

		Amide	Guanidino	Free water	MT	NOE (−3.5)
k_s (s^{-1})	LB–UB	1–250	1–1000	–	1–100	1–30
f_s (10^{-3})		0.1–10	1–50	–	10–400	10–100
$T_{2,s}$ (10^{-3} s)		0.1–10	0.1–10	20–100	0.01–0.3	0.1–10
Δ (ppm)		3.5	2	0	−2.4	−3.5

Table 1. Summary of the parameters for a general exchanging pool i when we conduct R_{ex} and AREX fitting: solute-water exchange rate (k_i), solute concentration (f_i), transverse relaxation time ($T_{2,s}$), and solute resonance frequency offset (Δ).

Define a set of LB and UB from Table 1, and start at the point $x_0 = LB + (UB - LB)/2$
The pixel-wise decompositions of R_{eff} and R_{ex} for CEST are solved by nonlinear fitting function (`lsqnonlin`) in MATLAB
Loop for Z-spectra of each pixel
{
compute R_{eff} and R_{ex} fitting parameters from Eqs. (2) and (3), respectively
compute Z-spectra of R_{ex}-line-fit from Eq. (1)
}
Obtain fitting parameters and reconstruct the R_{ex} imaging from Z-spectra of each pixel

Table 2. Pseudo-code of the R_{ex} based method for Z-spectra fitting and decomposition.

		Amide	Guanidyl/Amine	Amino	MT	NOE (−1.6)	NOE (−3.5)
A	LB–UB	0–10	0–10	0–10	0–40	0–10	0–20
W		0–3	0–3	0–3	0–35	0–3	0–10
Δ (ppm)		3.6	2	3	−1.5	−1.6	−3.5

Table 3. Summary of the parameters used for Lorentzian fitting: amplitude (A), width (W), and solute resonance frequency offset (Δ).

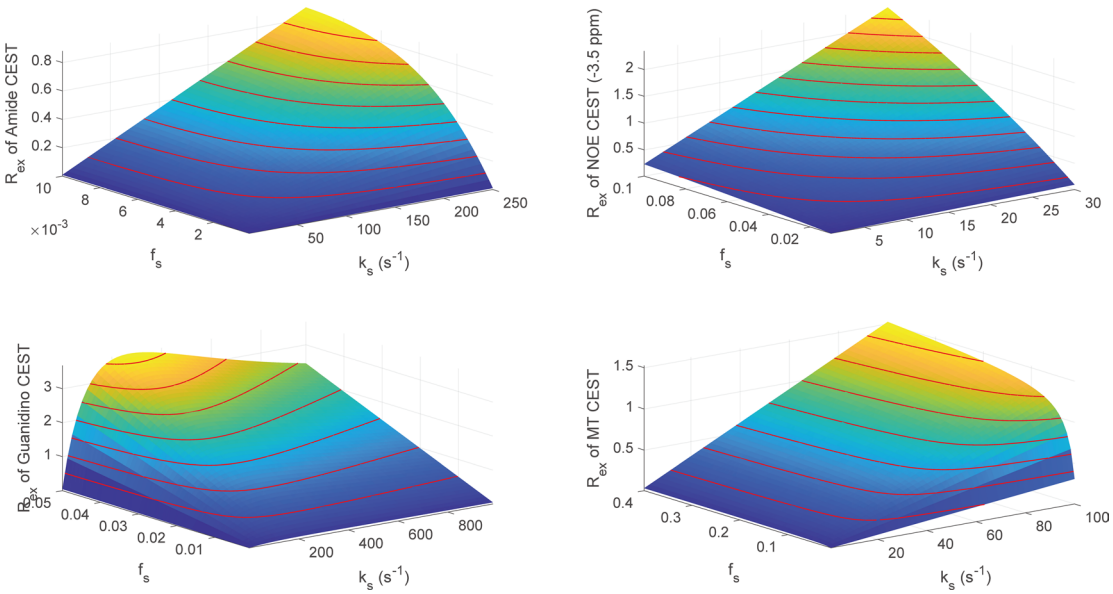

Fig. 2. The correlation between R_{ex} and parameters (k_s, f_s) for Amide, NOE (−3.5 ppm), Guanidino and MT. For each subplot, the red line denotes the contour.

separating CEST parameters. For Amide, NOE (− 3.5 ppm), Guanidino and MT, Fig. 2 illustrates the correlations between parameters (k_s, f_s) and R_{ex}. The surface plots demonstrate the dependence of R_{ex} on k_s and f_s, where R_{ex} is linear monotonically increasing with parameters (k_s, f_s) for the Amide, NOE (− 3.5 ppm) and Guanidino. For MT, its R_{ex} is linear monotonically increasing with solute concentration f_s, while a nonlinear monotonically increasing relationship between R_{ex} and solute-water exchange rate k_s is observed. It should be noted that the R_{ex} of Guanidino depicts a monotonically increasing trend first and then decrease corresponding to k_s, while its R_{ex} follows a monotonically increasing pattern in respect to f_s. In addition, R_{ex} is nonlinear monotonically increasing with $T_{2,s}$ for the Amide, NOE (-3.5 ppm) and Guanidino, while R_{ex} shows a trend of slight monotonic decrease corresponding to $T_{2,s}$ for MT, as illustrated in Fig. 3. In addition, Fig. 4 illustrates an example of R_{ex} changing with k_s and $R_{2,s}$ ($1/T_{2,s}$) for Amide, where R_{ex} follows a increasing pattern in respect to $R_{2,s}$ at different k_s and R_{ex} shows a trend of decrease corresponding k_s at different $R_{2,s}$.

R_{ex}, Lorentzian, and AREX imaging

Herein, we conduct an experiment of R_{ex}, Lorentzian and AREX imaging for Amide at 3.5 ppm, Guanidino at 2.0 ppm, MT at − 2.4 ppm and NOE at − 3.5 ppm, where each pixel of imaging is obtained by computing the peaks of R_{ex} and Lorentzian decompositions. Figure 5 illustrates the R_{ex}, Lorentzian and AREX imaging of these CEST effects. The region of pseudo color image overlaid on anatomy image is the region of interest (ROI), where the region of tumor region is marked with solid red contour and the solid red contour denotes the contralateral region. Visually, the R_{ex} shows different structure distributions on the R_{ex} imaging for Amide, Guanidino, MT and NOE, this is different from Lorentzian and AREX.

Figure 6 illustrate the Z-spectra fitting from the tumor region and the contralateral region using the R_{ex}, Lorentzian and AREX approach, respectively. The results show that the satisfied accuracy and consistency are obtained by the proposed R_{ex}-line-fit and it displays great agreement and follows the same tendency as the actual measurements. Table 4 lists the mean value and standard deviation of residual between the considered fitting approach and the experimental Z-spectra for the tumor region and its contralateral region.

We further applied the linear regression analysis[29] to assess the general performance of the R_{ex}, Lorentzian and AREX approach using the whole ROI data of CEST images at 49 frequency offsets. Figure 7 displays the R_{ex},

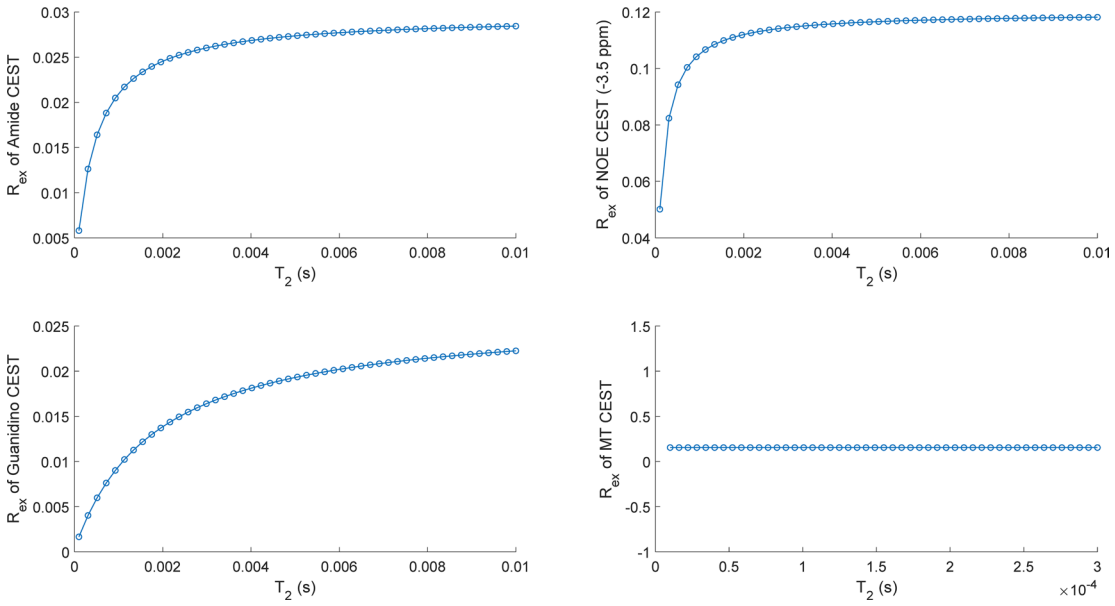

Fig. 3. The correlation between R_{ex} and $T_{2,s}$ for Amide, NOE (− 3.5 ppm), Guanidino and MT.

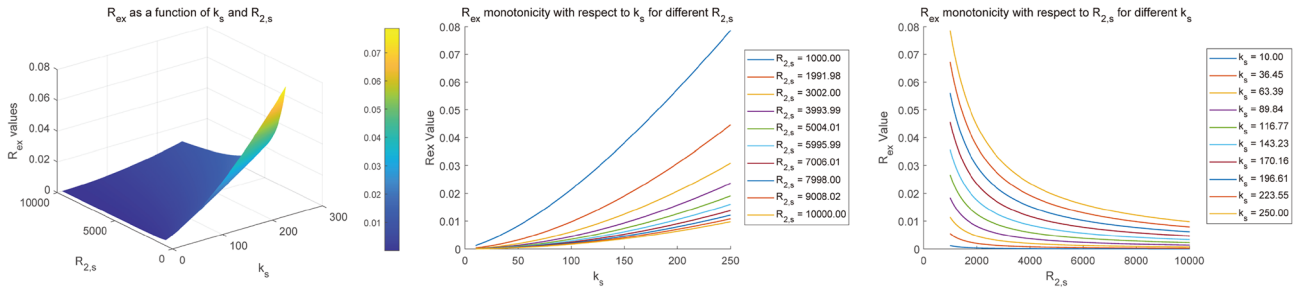

Fig. 4. An example of R_{ex} changing with k_s and $R_{2,s}$ ($1/T_{2,s}$) for Amide.

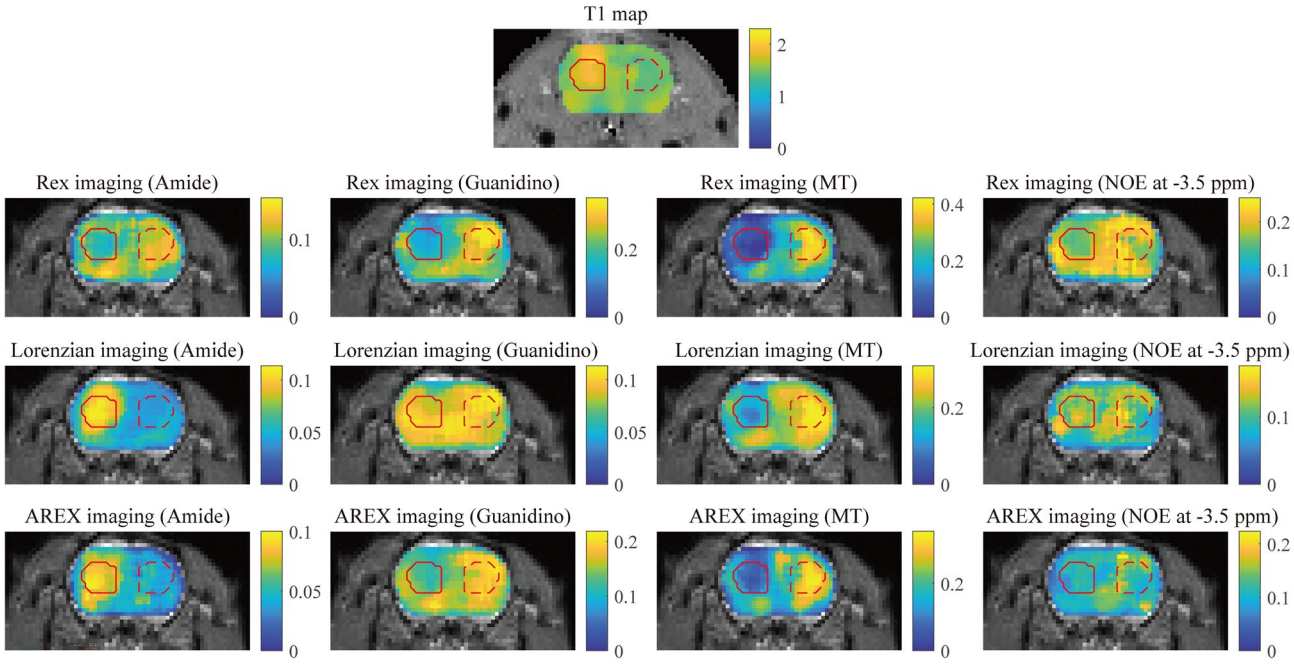

Fig. 5. The R_{ex}, Lorentzian and AREX imaging of Amide at 3.5 ppm, Guanidino at 2.0 ppm, MT at −2.4 ppm and NOE at −3.5 ppm. The solid red contour denotes the tumor region and the dashed red contour is the contralateral region.

Lorentzian and AREX for fitting CEST signal by plotting the linear regression lines between the experimentally acquired data and the fitting. The excellent performance of our R_{ex} method is confirmed by the scatter and linear regression lines, resulting in a very high coefficient of determination ($R^2 = 0.9937$).

Discussion

The exchange-dependent relaxation R_{ex} is an important parameter for CEST effects and can be used to determine the exchange rate k_s of the exchangeable protons with concentration fraction f_s and transverse relaxation $T_{2,s}$. In this study, we proposed a method that can support reliable quantitative separation of CEST effect by R_{ex}. This is important because specificity of in vivo CEST effect is challenging due to careful measurement of the CEST effects. Nevertheless, some discussions should be made as follows.

In the Eq. (4) of R_{ex}, the first term named 'k_i-term' is the dominant factor, which comprises the product of peaks for water pool ('a-peak') and CEST pool ('b-peak'), respectively. The '$R_{2,i}$-term', together with the 'b - peak', denotes the exchange dependent relaxation that yields an off-resonant peak in CEST. So the R_{ex} turns into two peaks, but unlike Lorentzian and AREX lineshape that gives only one peak. In fact, the effect of water T1 and T2 relaxation time on Lorentzian shape is described by formula in Ref.[17]. In contrast, R_{ex} excludes water T1 and T2 contributions, which serves as a tool for calculating the CEST signal, offering a more representative depiction of chemical exchange processes than traditional CEST analysis methods[30,31]. As a reduced form of R_{ex}, AREX is a Lorentzian function[28], excluding the water pool ('a-peak'), unlike the complete Rex expression[2,28]. It is interesting to study the 'a-peak' imaging, which will be presented in our next work.

In the R_{ex} imaging, the tumor regions marked with solid red contour show reduced values in correspondence with the contralateral regions (Fig. 5). In practice, the exchange rate k_i can be determined by analyzing the CEST signal as a function of pH: $k_{amide} = 5.57 \times 10^{pH-6.4}$, $k_{guanidyl} = 5.57 \times 10^{pH-6.4}$[32]. An intuitive explanation is that the reduced exchange rate with lower pH in and around the tumor region causes the lowering of the R_{ex} peak values (Fig. 6). In fact, the mechanism behind tumors is more complex compared with the clear process of stroke. Particularly, the R_{ex} mechanism is considered that many factors (the exchange rate k_s, the concentration fraction f_s and transverse relaxation $T_{2,s}$) participated in this process (Eq. 4). To some extent, the R_{ex} imaging shows the specificity for different chemical groups, because different structure distributions on the R_{ex} imaging for Amide, Guanidino, MT and NOE are obtained, this is different from multiple-pool Lorentzian, AREX and T_1 map (Fig. 5). Nevertheless, some multi-pool models have been applied to tumor research, such as Refs.[33,34].

In this study, we have made some meaningful explorations and obtained promising research results. We first determined whether parameters (solute-water exchange rate and solute concentration) and R_{ex} have a monotonous relationship for Amide at 3.5 ppm, Guanidino at 2.0 ppm and NOE at −3.5 ppm (Figs. 2, 3, 4). With this knowledge in mind, this makes it possible to isolate some part parameters by extending previous approaches, where numerical simulations of R_{ex} can be used to obtain saturation parameters for CEST effect.

We further implemented R_{ex} as a novel model to provide high-accuracy CEST fitting and decomposition where multiple CEST saturation transfer pools are present. The proposed R_{ex}-line-fit avoids specific selection of tissue parameters and minimizes operator bias, enabling adaptive fitting and decomposition for reliable estimation of CEST effects. The accuracy of R_{ex}-line-fit was first validated by the test of in vivo mouse, which revealed

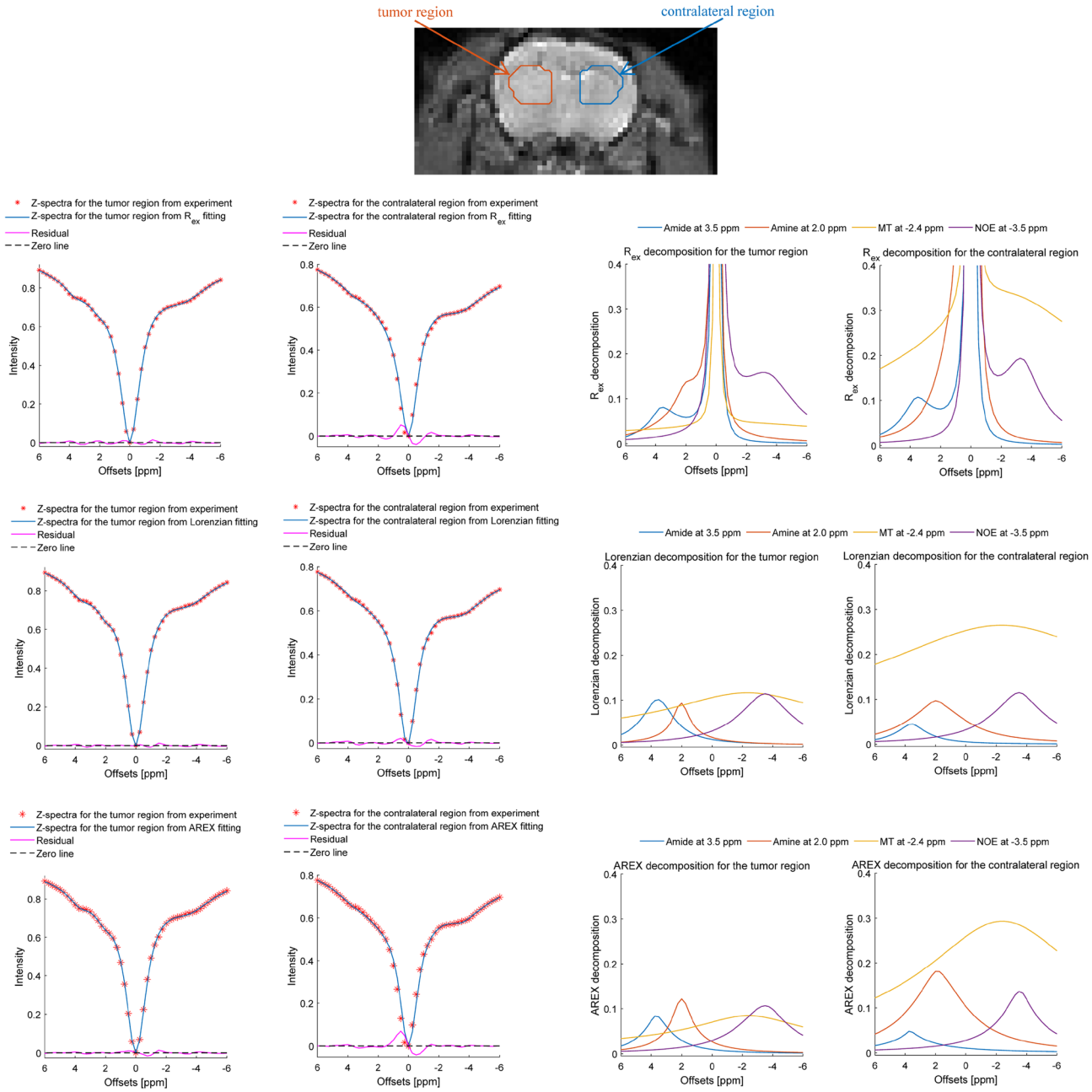

Fig. 6. Z-spectra fitting and decomposition from the tumor region and its contralateral region using the R_{ex}, Lorentzian and AREX approaches.

	Residual between R_{ex} fitting and the experimental Z-spectra		Residual between Lorentzian fitting and the experimental Z-spectra		Residual between AREX fitting and the experimental Z-spectra	
Mean value	1.8914×10^{-4}	3.8786×10^{-4}	-1.3783×10^{-5}	1.7531×10^{-5}	2.6252×10^{-5}	1.2×10^{-3}
Standard deviation	0.0054	0.0147	0.0043	0.0070	0.0053	0.0183
	Tumor region	Contralateral region	Tumor region	Contralateral region	Tumor region	Contralateral region

Table 4. The mean value and standard deviation of residual between the considered fitting approach and the experimental Z-spectra for the tumor region and its contralateral region.

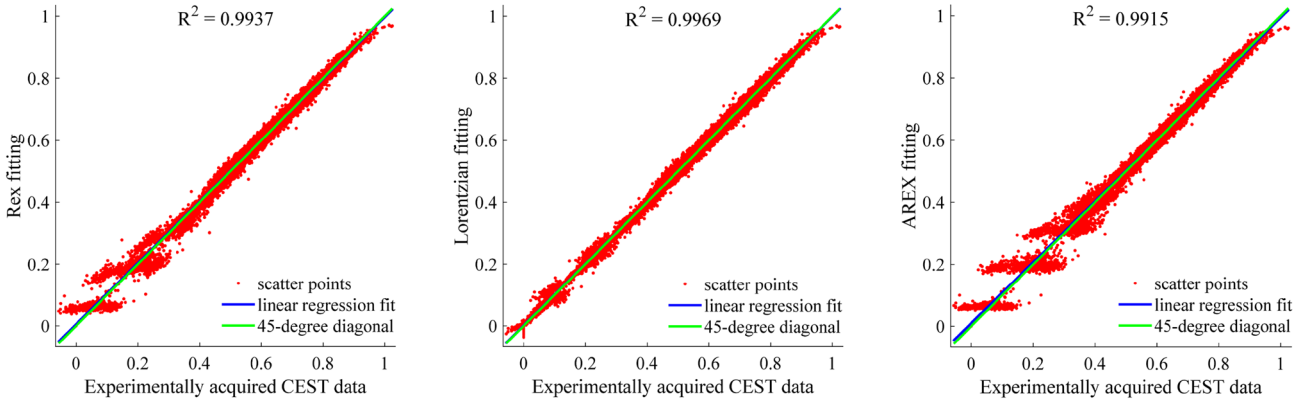

Fig. 7. Linear regression analysis of the R_{ex}, Lorentzian and AREX fitting when they compared with the experimentally acquired data within the ROI.

that R_{ex} method provided a near-perfect approximation to the experimentally acquired Z-spectra (Table 4, Figs. 6 and 7).

Conclusion

As an improvement method that only is dependent of the specific parameters (solute concentration, solute-water exchange rate, solute transverse relaxation, and irradiation power), our R_{ex}-line-fit can provide a simple, robust and more accurate approach for approximating CEST and further serve for quantitative separation of CEST effect. More in vivo validations and at the clinical field strength will be performed in the future.

Data availability

The datasets used and/or analysed during the current study available from the corresponding author on reasonable request.

Received: 15 January 2024; Accepted: 4 September 2024
Published online: 14 September 2024

References

1. Kogan, F., Hariharan, H. & Reddy, R. Chemical exchange saturation transfer (CEST) imaging: Description of technique and potential clinical applications. *Curr. Radiol. Rep.* **1**, 102–114 (2013).
2. Zaiss, M. & Bachert, P. Chemical exchange saturation transfer (CEST) and MR Z-spectroscopy in vivo: A review of theoretical approaches and methods. *Phys. Med. Biol.* **58**(22), R221 (2013).
3. El Mamoune, K. *et al.* Application of chemical exchange saturation transfer (CEST) in neuroimaging. *J. Chem. Neuroanat.* **114**, 101944 (2021).
4. Zaiss, M. *et al.* Theory of chemical exchange saturation transfer MRI in the context of different magnetic fields. *NMR Biomed.* **35**(11), e4789 (2022).
5. Van Zijl, P. C. & Yadav, N. N. Chemical exchange saturation transfer (CEST): What is in a name and what isn't?. *Magn. Reson. Med.* **65**(4), 927–948 (2011).
6. Song, X. *et al.* CEST phase mapping using a length and offset varied saturation (LOVARS) scheme. *Magn. Reson. Med.* **68**(4), 1074–1086 (2012).
7. Liu, G. *et al.* Nuts and bolts of chemical exchange saturation transfer MRI. *NMR Biomed.* **26**(7), 810–828 (2013).
8. Pankowska, A. *et al.* Chemical exchange saturation transfer (CEST) as a new method of signal obtainment in magnetic resonance molecular imaging in clinical and research practice. *Pol. J. Radiol.* **84**, e147 (2019).
9. Zhang, L. *et al.* Voxel-wise Optimization of Pseudo Voigt Profile (VOPVP) for Z-spectra fitting in chemical exchange saturation transfer (CEST) MRI. *Quant. Imaging Med. Surg.* **9**(10), 1714 (2019).
10. Liu, Y. *et al.* Dual-Peak Lorentzian CEST MRI for antiretroviral drug brain distribution. *Neuroimmune Pharmacol. Therap.* **2**(1), 63–69 (2023).
11. Windschuh, J. *et al.* Correction of B1-inhomogeneities for relaxation-compensated CEST imaging at 7 T. *NMR Biomed.* **28**(5), 529–537 (2015).
12. Desmond, K. L., Moosvi, F. & Stanisz, G. J. Mapping of amide, amine, and aliphatic peaks in the CEST spectra of murine xenografts at 7 T. *Magn. Reson. Med.* **71**(5), 1841–1853 (2014).
13. Cai, K. *et al.* CEST signal at 2 ppm (CEST@ 2 ppm) from Z-spectral fitting correlates with creatine distribution in brain tumor. *NMR Biomed.* **28**(1), 1–8 (2015).
14. Bade, A. N. *et al.* Chemical exchange saturation transfer for detection of antiretroviral drugs in brain tissue. *Aids* **35**(11), 1733–1741 (2021).
15. Tietze, A. *et al.* Assessment of ischemic penumbra in patients with hyperacute stroke using amide proton transfer (APT) chemical exchange saturation transfer (CEST) MRI. *NMR Biomed.* **27**(2), 163–174 (2014).
16. Zhang, X. Y. *et al.* Accuracy in the quantification of chemical exchange saturation transfer (CEST) and relayed nuclear Overhauser enhancement (rNOE) saturation transfer effects. *NMR Biomed.* **30**(7), e3716 (2017).
17. Zaiß, M., Schmitt, B. & Bachert, P. Quantitative separation of CEST effect from magnetization transfer and spillover effects by Lorentzian-line-fit analysis of z-spectra. *J. Magnet. Resonance* **211**(2), 149–155 (2011).
18. Glang, F. *et al.* DeepCEST 3T: Robust MRI parameter determination and uncertainty quantification with neural networks—Application to CEST imaging of the human brain at 3T. *Magnet. Resonance Med.* **84**(1), 450–466 (2020).
19. Wu, Y. *et al.* 3D APT and NOE CEST-MRI of healthy volunteers and patients with non-enhancing glioma at 3 T. *Magnet. Resonance Mater. Phys. Biol. Med.* **35**(1), 63–73 (2022).

20. Cui, J., Sun, C. & Zu, Z. NOE-weighted imaging in tumors using low-duty-cycle 2π-CEST. *Magnet. Resonance Med.* **89**(2), 636–651 (2023).
21. Zhao, Y., Sun, C. & Zu, Z. Assignment of molecular origins of NOE signal at − 3.5 ppm in the brain. *Magnet. Resonance Med.* **90**(2), 673–685 (2023).
22. Cui, J. *et al.* Evaluation of contributors to amide proton transfer–weighted imaging and nuclear Overhauser enhancement–weighted imaging contrast in tumors at a high magnetic field. *Magnet. Resonance Med.* **90**(2), 596–614 (2023).
23. Chen, L. *et al.* Creatine and phosphocreatine mapping of mouse skeletal muscle by a polynomial and Lorentzian line-shape fitting CEST method. *Magnet. Resonance Med.* **81**(1), 69–78 (2019).
24. Carradus, A. J. *et al.* Measuring chemical exchange saturation transfer exchange rates in the human brain using a particle swarm optimisation algorithm. *NMR Biomed.* **36**(11), e5001 (2023).
25. Cui, J., Afzal, A. & Zu, Z. Comparative evaluation of polynomial and Lorentzian lineshape-fitted amine CEST imaging in acute ischemic stroke. *Magnet. Resonance Med.* **87**(2), 837–849 (2022).
26. Khlebnikov, V. *et al.* On the transmit field inhomogeneity correction of relaxation-compensated amide and NOE CEST effects at 7 T. *NMR Biomed.* **30**(5), e3687 (2017).
27. Xiao, G. *et al.* Deep learning to reconstruct quasi-steady-state chemical exchange saturation transfer from a non-steady-state experiment. *NMR Biomed.* **36**(9), e4940 (2023).
28. Zhang, X. Y. *et al.* Increased CEST specificity for amide and fast-exchanging amine protons using exchange-dependent relaxation rate. *NMR Biomed.* **31**(2), e3863 (2018).
29. Li, Y. *et al.* Accelerating GluCEST imaging using deep learning for B0 correction. *Magnet. Resonance Med.* **84**(4), 1724–1733 (2020).
30. Zaiss, M. *et al.* Inverse Z-spectrum analysis for spillover-, MT-, and T1-corrected steady-state pulsed CEST-MRI-application to pH-weighted MRI of acute stroke. *NMR Biomed.* **27**(3), 240–252 (2014).
31. Zaiss, M. *et al.* Relaxation-compensated CEST-MRI of the human brain at 7 T: Unbiased insight into NOE and amide signal changes in human glioblastoma. *Neuroimage* **112**, 180–188 (2015).
32. Jin, T. *et al.* Enhancing sensitivity of pH-weighted MRI with combination of amide and guanidyl CEST. *Neuroimage* **157**, 341–350 (2017).
33. Zhou, I. Y. *et al.* Quantitative chemical exchange saturation transfer (CEST) MRI of glioma using Image Downsampling Expedited Adaptive Least-squares (IDEAL) fitting. *Sci. Rep.* **7**(1), 84 (2017).
34. Rivlin, M. *et al.* Breast cancer imaging with glucosamine CEST (chemical exchange saturation transfer) MRI: First human experience. *Eur. Radiol.* **32**(11), 7365–7373 (2022).

Author contributions

GX: Conceptualization, Methodology, Software; X.-L.Z: Methodology, Formal analysis, Investigation, Validation, Visualization, Writing – original draft; S.-Q.W: Formal analysis, Data curation; S.-X.L: Formal analysis, Data curation; T.-T.N: Resources, Data curation; Y.-W.C: Investigation, Supervision; C.-Y.Z: Resources, Data curation; GY: Investigation, Supervision, Writing – review & editing; R.-H.W: Funding acquisition, Project administration, Writing – review & editing.

Funding

The study was supported by the National Natural Science Foundation of China (Grant/Award Number: 82020108016), the Grant for Key Disciplinary Project of Clinical Medicine under the Guangdong High-Level University Development Program (Grant/Award Number: 002-18120302), the Functional Substances in Medicinal Edible Resources and Healthcare Products (Grant/Award Number: 2021B1212040015), the 2021 Medical Research Foundation of Guangdong (Grant/Award Number: 202011102275838), the 2021 Grant for Key Science Technology and Innovation Project under the Guangdong Jieyang Development Program (Grant/Award Number: 210517084612609), and the Medical Health Science and Technology Project of Shantou (Grant/Award Number: 2022-88-16).

Competing interests

The authors declare no competing interests.

Additional information

Correspondence and requests for materials should be addressed to G.Y. or R.-H.W.